Thermodynamics of Liquid (Xenon + Methane) Mixtures

Lino M. B. Dias,[†,‡] Eduardo J. M. Filipe,[†] Clare McCabe,[§] and Jorge C. G. Calado*[,†]

Centro de Química Estrutural, Instituto Superior Técnico, 1049-001 Lisboa, Portugal, and Department of Chemical Engineering, Colorado School of Mines, Golden, Colorado 80401

Received: October 10, 2003; In Final Form: February 10, 2004

A new apparatus for the study of vapor−liquid or vapor−liquid−liquid equilibrium has been assembled. The apparatus, based on a static and analytical method, can perform measurements at temperatures from 185 to 320 K and pressures up to 8 MPa. The equilibrium vapor pressures of (xenon + methane) binary mixtures have been measured at seven temperatures, from 189.78 to 273.18 K, and at pressures up to 6.8 MPa. The mixture critical line has been estimated and found to be continuous between the critical points of the pure components. The system is found to display type I behavior in the classification scheme of Scott and van Konynenburg. The results have been correlated by the Peng−Robinson equation of state and a more rigorous theoretical study performed with the statistical associating fluid theory for potentials of variable range (SAFT-VR).

1. Introduction

Twenty years after the publication of the seminal book by Rowlinson and Swinton, *Liquids and Liquid Mixtures*,[1] there is still a need for good experimental data on a certain number of model systems. Given the fact that a whole array of molecular features—size, shape, flexibility, etc—contribute to the thermodynamic behavior of a liquid mixture, it is useful to look at families or series of systems so that trends can be detected and correlations explored. Among the first to be studied were mixtures of spherical and quasi-spherical molecules. Typical examples of the former are the noble gases, and an obvious choice for the latter is methane. Detailed thermodynamic studies of liquid mixtures of methane with both argon[1] and krypton[2] have been published. (Krypton and methane have, in fact, very similar sizes and interaction energies, leading to the almost ideal behavior of (krypton + methane) mixtures.[2]) A whole series of mixtures of xenon with light alkanes, viz., ethane, propane, *n*-butane, and *i*-butane, have also been investigated. (Only methane is missing from the list.) It thus seemed worthwhile to study the (xenon + methane) system, the missing link between those series (of methane with the noble gases and of xenon with the lower alkanes). As far as we are aware, no liquid−vapor equilibrium study has been performed on such system. The reason is obvious: unlike the other mixtures in the two families of systems, which can be studied at low pressures, the liquid overlap of xenon and methane happens at moderately high pressures. (The vapor pressure of methane at the xenon triple point is 16 bars.)

From a theoretical point of view, a major development in our understanding of liquid mixtures has been the emergence in the late 1980s of molecularly based equations of state (EOS) such as the statistical associating fluid theory (SAFT).[3,4] Molecularly based EOSs provide a suitable framework within which the effects of molecular shape and interactions on the thermodynamic properties can be separated and quantified. Each contribution depends on molecular parameters that have a physical meaning, such as the size of the molecule or the nature of functional groups comprising it. An important feature of SAFT is that it explicitly takes into account nonsphericity and association interactions, thus providing a powerful method for studying the phase behavior of chain molecules.

In previous papers in this series,[5,6] we have reported results on the excess thermodynamic properties of simple liquid mixtures of xenon with the lower alkanes, namely, ethane, propane, *n*-butane, and *i*-butane. Whereas the general aim of the project was to investigate the role of molecular shape (and shape-related properties such as polarity) on the thermodynamic behavior of the system, the observation that the (xenon + ethane) mixtures exhibit negative values for all four major excess functions (G^E_m, H^E_m, S^E_m, and V^E_m) suggested at first a relatively strong interaction between xenon and the alkane molecule. Subsequently, however, we were able to show that the peculiar excess functions exhibited by these systems were due to an unexpected similarity, at least in terms of phase equilibria, between xenon and the *n*-alkanes. Using the statistical associating fluid theory, the experimental results could be interpreted at the molecular level in terms of size and molecular interactions. To summarize, we have found that the SAFT parameters obtained for xenon lie within the average value of those used to describe the *n*-alkanes, implying that xenon can be represented as a sphere with almost the same diameter and potential as those suited to describe the *n*-alkanes. Ultimately, this also implies that mixtures of (xenon + *n*-alkane) can be thought as a particular case of mixtures of the *n*-alkanes. Indeed, it is found that mixtures of *n*-alkanes, except for those involving methane, do deviate negatively from Raoult's law and exhibit negative excess Gibbs energies and negative excess volumes. Furthermore, it was found that the (xenon + *n*-alkane) mixtures follow the Lorentz−Berthelot combining rules so that no unlike interaction parameters are fit to experimental mixture data, enabling the use of the theory in a totally predictive way.[5,6] Subsequent studies have also shown that in general the behavior of mixtures of an *n*-alkane with a second component is mirrored

* Corresponding author. E-mail: jcalado@ist.utl.pt.
† Instituto Superior Técnico.
‡ Present address: Bayer Technology Services GmbH, Process Management Technology, SCL-SCO, 51368 Leverkusen, Germany.
§ Colorado School of Mines.

10.1021/jp037070n CCC: $27.50
Published on Web 05/05/2004

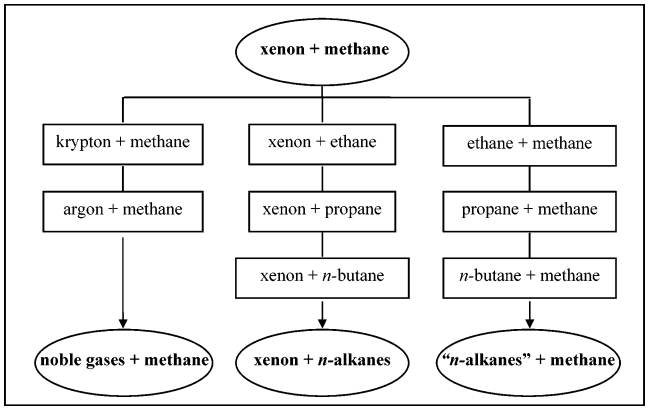

Figure 1. Schematic illustration the central role of the xenon + methane system.

by that of xenon with that same component.[7] Finally, we have found that in binary mixtures where deviations from the Lorentz−Berthelot combining rules occur the unlike interaction parameter can be used interchangeably between mixtures involving xenon and those involving alkanes, eliminating the need to fit to experimental mixture data.[7]

In summary, the (xenon + methane) system occupies a unique position at which several series of systems converge (Figure 1), and for that reason its study is of particular interest. A new experimental apparatus was assembled for this purpose. Vapor−liquid equilibrium measurements were performed at seven temperatures between 189.78 and 273.18 K, which essentially corresponds to the range of temperatures between the critical points of the pure components. The lowest temperature, 189.78 K, lies only 0.6 K below the critical temperature of methane (190.4 K) and 28 K above the triple point of xenon (161.40 K), whereas the highest, 273.18 K, is 16.5 K below the critical temperature of xenon. Because of experimental constraints, no measurements were performed at lower temperatures. The mixture critical line was located and found to be continuous between the critical points of the pure components. The system is found to display type I behavior in the classification scheme of van Konynenburg and Scott.[8]

As in the previous studies, the phase equilibria results were interpreted using the statistical associating fluid theory for potentials of variable range (SAFT-VR). We have found that the (xenon + methane) mixtures conform to the Lorentz−Berthelot combining rules for the unlike interaction and the theoretical results accurately predict the experimental results. SAFT-VR also confirms the type I classification for the (methane + xenon) phase diagram.

2. Experimental Section

The experimental measurements were performed in a new apparatus recently assembled for the study of vapor−liquid or vapor−liquid−liquid equilibrium. The apparatus makes use of a static and analytical method and can perform measurements at temperatures from 185 to 320 K and pressures up to 8 MPa. Its design was based on the equipment used by Streett[9] and co-workers.

A schematic diagram of the apparatus is shown in Figure 2. Basically it consists of a thick-walled glass cell of approximately 13.6-cm^3 capacity, immersed in a commercial cryogenic bath. The glass cell has the advantage of allowing a visual detection of the vapor−liquid critical line of the mixture, thanks to the characteristic opalescence observed near the critical point, but sets an upper limit to the pressure range of about 8 MPa.

Temperature was measured with a platinum 100-Ω resistance thermometer, associated with a Prema 6031 multimeter. The setup was calibrated (ITS-90) against a standard platinum 25-Ω resistance thermometer (which in turn had been calibrated in the 177−693 K range against several fixed-point temperatures). The final reading accuracy lies within ±0.01 K. The vapor pressures were measured using a Setra 205-2 transducer, associated with a Prema 6001 multimeter. This measuring set was calibrated against a Ruska Instrument Corporation dead-weight gauge (model 2417). The final pressure reading accuracy lies within ±1.3 kPa throughout the entire pressure range (up to 7 MPa).

The components are condensed directly into the equilibrium cell from the gas cylinders. The more volatile component should be the second to be introduced. Mixing of the two components is facilitated by a Teflon-coated stirrer operated by an immersed magnet. The connecting lines between the equilibrium cell and the pressure transducer are made of 0.76-mm i.d. ($^1/_8$" e.d.) stainless steel tubing and were kept at a higher temperature (relative to the temperature of the cell) to avoid undesirable condensations. The total volume of these lines is therefore very small compared to the total volume of the vapor phase. Capillary lines made of 0.76-mm i.d. ($^1/_8$" e.d.) stainless steel tubing are used to withdraw small samples of liquid and vapor after equilibrium between the two phases has been reached, confirmed by the constancy of the pressure readings. The sampling tube for the liquid phase(s) can be moved upward and downward so as to reach any level in the cell. This will become important when more than one liquid phase is present (not the present case). The samples are analyzed by a differential thermal conductivity method, using a catherometer (Gow-Mac 10.747-I) kept at a constant temperature in an ice bath, to improve stability. The readings were made using a Prema 6001 multimeter and the input current of the thermal conductivity cell supplied by a Hewlett Packard 6920B current stabilizer (±0.0005 V) monitored by a Keithley 191 multimeter. The detector was previously calibrated using binary gaseous mixtures of known composition. These were prepared in 0.2-dm^3 stainless steel cylinders, held at 298.15 ± 0.01 K, by the partial pressure addition of each component up to a total pressure of about 1 bar (measured by a Paroscientific Digiquartz 6100A pressure transducer). The sensitivity of the analyzer that depends, among other factors, on the difference between the thermal conductivities of the two components, is on the order of 0.0009 mole fraction in the present case. However, errors associated with sampling and the calibration process bring the reproducibility of the results to ±0.003 mole fraction.

The gases were from Air Liquide, and both had a stated purity of 0.99995 mass fraction. They were used without further purification. The vapor pressure of pure CH_4 was measured in the 184−190 K range and was found to agree, within 0.3%, with the literature data.[10] The vapor pressure of pure xenon was also measured between 189 and 283 K. The overall agreement with the values of Theeuwes and Bearman[11] is within 0.3% for most of the range, increasing to 0.6% at the lower limit. This difference can be accounted for by temperature differences smaller than ±0.04 K, well within the bath temperature stability in this range.

3. Results

The equilibrium vapor pressure and composition results (p, T, x, y) of (xenon + methane) mixtures at each temperature are recorded in Table 1 and plotted in Figure 3. All isotherms except one are in the critical region. The exception is the 189.78 K

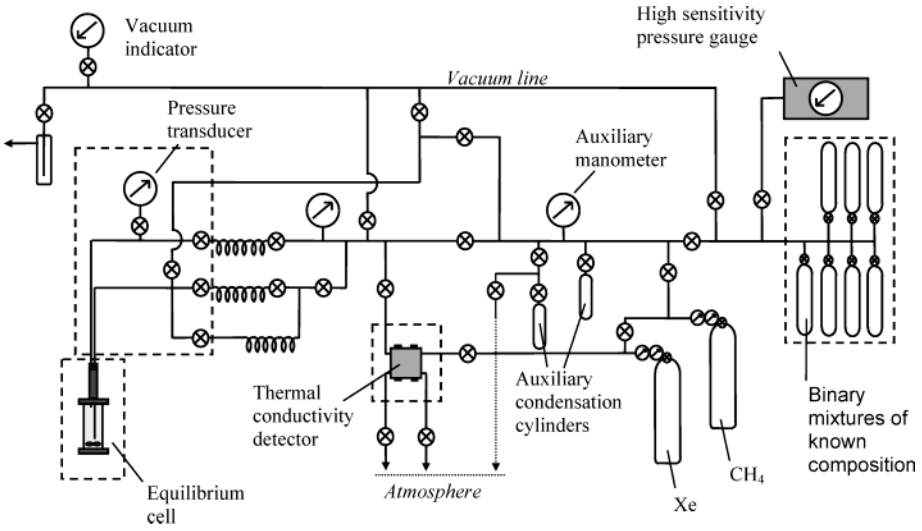

Figure 2. Schematic representation of the experimental apparatus.

TABLE 1: Vapor Pressures *p* of {*x*CH_4 + (1 − *x*)Xe} from 189.78 to 273.18 K[a]

p/MPa	*x*(CH_4)	*y*(CH_4)	*p*/MPa	*x*(CH_4)	*y*(CH_4)
	189.78 K		3.804	0.2318	0.5119
0.345	0	0	4.559	0.3317	0.5778
0.693	0.0880	0.4877	5.290	0.4183	0.6165
1.128	0.1994	0.6913	5.927	0.4816	0.6355
1.592	0.3239	0.7850	6.217	0.5271	0.6373
2.073	0.4792	0.8348	6.370	0.5505	0.6268
2.632	0.6186	0.8800	*6.60*	*0.61*	*0.61*
3.231	0.7645	0.9214			
3.743	0.8822	0.9470		**248.15 K**	
4.487	1	1	2.312	0	0
			3.109	0.0706	0.2226
	208.29 K		4.020	0.1591	0.3733
0.705	0	0	4.895	0.2545	0.4563
1.174	0.0753	0.3789	5.482	0.3086	0.4947
1.814	0.1845	0.5928	5.976	0.3600	0.5145
2.411	0.2871	0.6908	6.292	0.3994	0.5191
3.018	0.4017	0.7484	6.419	0.4198	0.5203
3.617	0.5089	0.7879	*6.78*	*0.49*	*0.49*
4.234	0.6267	0.8203			
4.713	0.7122	0.8390		**260.62 K**	
5.001	0.7573	0.8486	3.127	0	0
5.231	0.7849	0.8532	3.617	0.0417	0.1108
5.426	0.8102	0.8594	4.213	0.0915	0.2124
5.65	*0.85*	*0.85*	4.733	0.1312	0.2771
			5.105	0.1678	0.3123
	223.81 K		5.624	0.2177	0.3521
1.182	0	0	6.092	0.2572	0.3769
1.726	0.0670	0.2961	6.305	0.2810	0.3834
2.345	0.1477	0.4713	6.393	0.2952	0.3834
2.961	0.2444	0.5716	*6.74*	*0.36*	*0.36*
3.656	0.3264	0.6508			
4.330	0.4353	0.6887		**273.18 K**	
4.934	0.5272	0.7256	4.137	0	0
5.017	0.5304	0.7281	4.574	0.0336	0.0693
5.516	0.5948	0.7376	5.021	0.0657	0.1288
5.841	0.6452	0.7398	5.441	0.1013	0.1745
6.20	*0.73*	*0.73*	5.720	0.1227	0.1969
			5.899	0.1361	0.2094
	236.17 K		6.056	0.1504	0.2175
1.686	0	0	6.287	0.1722	0.2256
2.426	0.0775	0.2732	*6.54*	*0.21*	*0.21*
3.121	0.1510	0.4201			

[a] *x* is the CH_4 mole fraction in the liquid phase; *y* is the CH_4 mole fraction in the vapor phase. For each isotherm, the critical point is shown in italics.

isotherm, which lies only 0.6 K below the critical temperature of the more volatile component, methane. The internal consistency of the data can be assessed in Figure 4 with the aid of the K_i value plots ($K_i = y_i/x_i$ where y_i is the mole fraction of component *i* in the vapor phase and x_i is the corresponding mole fraction in the liquid phase), which tend to exaggerate the scatter in the results. These plots are also useful when it comes to defining the mixture critical line: above the critical temperature of methane, the two branches converge and exhibit a vertical

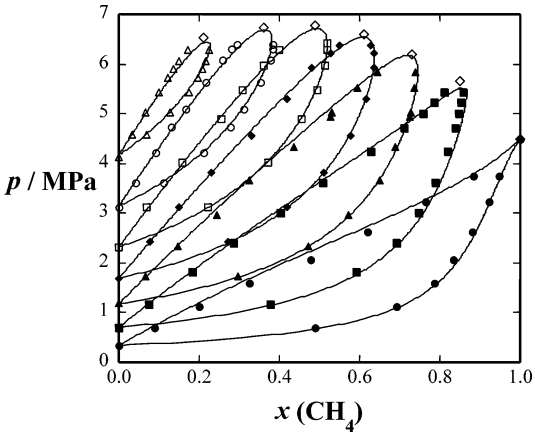

Figure 3. Constant-temperature *(P, x, y)* slices of the (methane + xenon) phase diagram. Solid lines correspond to the results obtained with the Peng−Robinson equation of state, and the symbols correspond to the experimental data given in Table 1. (△) 273.18, (○) 260.62, (□) 248.15, (◆) 236.17, (▲) 223.81, (■) 208.29, and (●) 189.78 K.

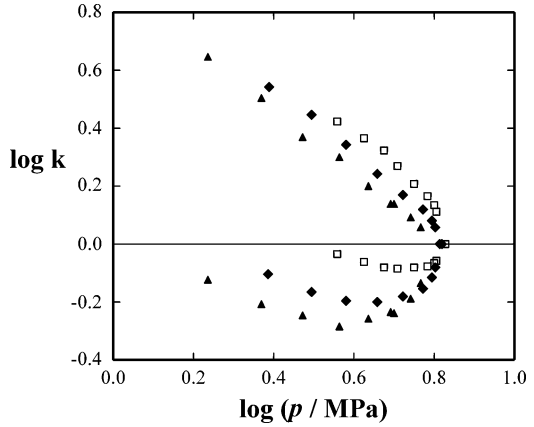

Figure 4. *K* diagram for three temperatures of the (xenon + methane) phase equilibria. (▲) 223.81, (◆) 236.17, and (□) 248.15 K.

tangent at the mixture critical point, where $K = 1$. The (xenon + methane) critical line is shown in Figure 6. For each isotherm, the critical state can be confirmed visually, thanks to its characteristic opalescence. The addition of a small quantity of one of the pure components brings the mixture to a one-phase transparent supercritical fluid. With a continuous critical line between the critical points of the pure components, the system belongs in type I (according to the classification of Scott and van Konynenburg for phase behavior). The occurrence of the liquid−liquid phase separation at lower temperatures is highly improbable.

4. Discussion

Given the simplicity of the molecules involved in this study and of the phase diagram obtained, a first attempt to correlate the experimental results was made using a simple equation, such as the Peng−Robinson equation of state.

$$p = \frac{RT}{V-b} - \frac{a(T)}{V(V+b)} + b(V-b) \qquad (1)$$

The pure-component parameters were evaluated from critical data, and the temperature dependence of constant a was evaluated from an expression based on Pitzer's acentric factor. For the concentration dependence of the a and b parameters on the van der Waals quadratic mixing rules was followed. The binary interaction parameter k_{12} was calculated from a best fit to the isotherm at 236.17 K, the midpoint of the experimental temperature range. The results are plotted in Figure 3 and show that the PR-EOS is able to make a good prediction of the experimental results at temperatures other than that used to fit k_{12}.

A quantitative interpretation of the results was performed using the statistical associating fluid theory for potentials of variable attractive range, SAFT-VR.[12,13] The main expressions of the SAFT-VR theory for the square-well potential have been presented,[5] and the reader is directed to the original references for full details.[12,13] In the SAFT-VR approach, molecules are described as chains of m tangent hard spherical segments with the attractive interactions modeled by a potential of variable attractive range, such as the square-well potential used in this work. Each segment is characterized by three parameters, namely, the hard-sphere diameter σ, the depth ϵ, and the width λ of the potential well. For the n-alkanes, a simple empirical relationship between the number of carbon atoms n in the alkyl chain and the number of spherical segments m in the model chain has been proposed in earlier work:

$$m = 1 + \left(\frac{n-1}{3}\right)$$

A single sphere is therefore used to model both the methane molecule and the xenon atom. The remaining pure-substance parameters, σ, ϵ and λ, are determined by fitting the theoretical expressions to the experimental vapor pressure and saturated liquid density data from the triple point to the critical point. As with all analytical equations of state, SAFT-VR overpredicts the experimental critical point because of the classical description of the critical region. Because in this work we are interested in the critical region of the phase diagram, the optimized parameters were rescaled to the experimental critical point.[14] The parameters used in this work are listed in Table 2, and the Lorentz−Berthelot combining rules were used to determine the unlike interactions. In this way, the SAFT-VR approach becomes completely predictive in the sense that no experimental results for the mixtures are needed. All calculations can be performed using solely pure-component parameters.

TABLE 2: Optimized Square-Well Intermolecular Potential Parameters for Methane and Xenon[a]

substance	m	σ/nm	$\epsilon/k(K^{-1})$	λ
CH_4	1.0	0.4069	157.4	1.444
Xe[6]	1.0	0.4243	225.9	1.478

[a] m is the number of spherical segments in the model, λ is the range parameter, σ is the diameter of each segment, and ϵ/k is the well depth.

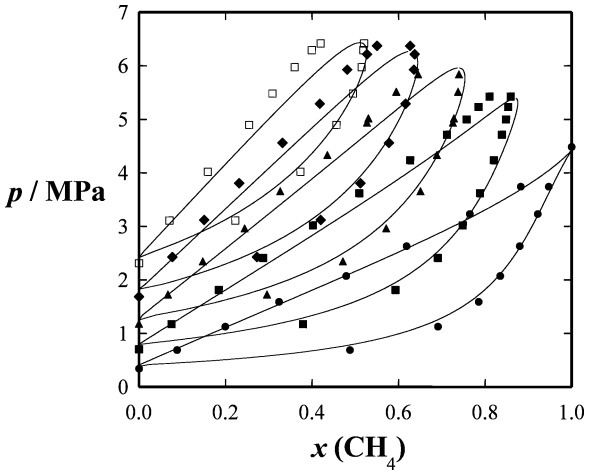

Figure 5. Constant-temperature *(P, x, y)* slices of the (methane + xenon) phase diagram. Solid lines correspond to predictions obtained from the SAFT-VR equation of state, and the symbols correspond to experimental data from Table 1. (□) 248.15, (◆) 236.17, (▲) 223.81, (■) 208.29, and (●) 189.78 K.

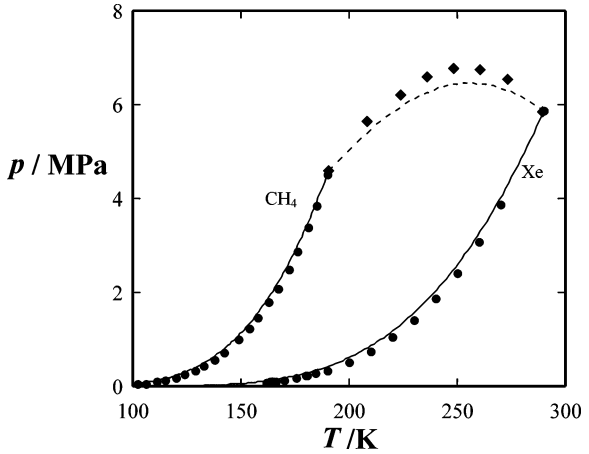

Figure 6. $p-T$ projection of the (xenon + methane) phase diagram as predicted by the SAFT-VR approach. Continuous lines represent the theoretical predictions, and symbols represent experimental data.[15]

Constant-temperature $p-x-y$ slices of the (xenon + methane) phase diagrams are presented in Figure 5, showing very good agreement with the experimental data. Both phase compositions are well described, as is the temperature dependence and the mixture critical line. In Figure 6, the $p-T$ projection of the phase diagram (as predicted by the SAFT-VR approach) is displayed and compared with the experimental data. The theory confirms type I behavior for the (xenon + methane) system.

The $p-T$ projection of the critical line for the (xenon + methane) mixture is plotted in Figure 7, together with those for the (methane + ethane)[15] and (xenon + ethane)[16] systems. Much to our surprise, the critical pressure and temperature of xenon fall, within experimental error, on the (methane + ethane) critical line. Even more interestingly, the whole (xenon +

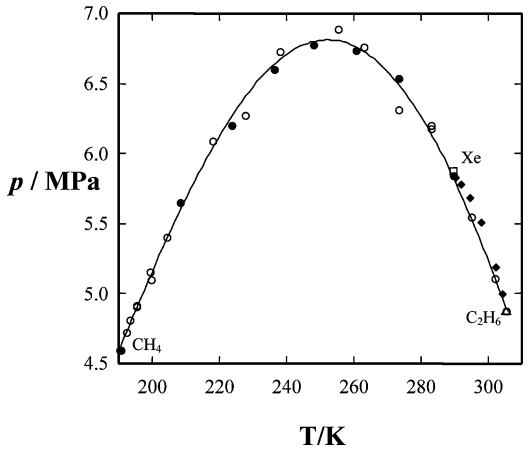

Figure 7. $p-T$ projection of the critical line for the (xenon + methane) (●) binary mixture compared to the critical loci of the (methane + ethane) (○) and (xenon + ethane) (◆) binary systems. Symbols correspond to experimental data,[15,16] and the continuous line is a smooth curve through the (methane + ethane) experimental data.

methane) critical curve matches, within experimental accuracy, the (methane + ethane) critical line, and so does that of the (xenon + ethane) mixture. In terms of phase equilibria, xenon behaves like a hypothetical mixture of methane and ethane. A simultaneous fit of the p_c versus x and T_c versus x projections of the (methane + ethane) critical line allows the estimation of this virtual composition. As far as phase diagrams are concerned, xenon behaves like a (methane + ethane) mixture with a methane mole fraction of $x = 0.179$. This interesting result raises all sorts of questions: (i) How will the vapor pressure of a (0.179 methane + 0.821 ethane) liquid mixture compare with the corresponding vapor pressure of xenon? (ii) Will a mixture of critical xenon and critical (0.179 methane + 0.821 ethane) still be critical? (iii) What type of critical behavior will the (xenon + methane + ethane) ternary system show? Some of these questions will be dealt with in future work.

Acknowledgment. L.M.B.D. thanks the Fundação para a Ciência e a Tecnologia (FCT) for financial support.

References and Notes

(1) Rowlinson, J. S.; Swinton, F. L. *Liquids and Liquid Mixtures*, 3rd ed., Butterworth Scientific: London, 1982.
(2) Calado, J. C. G.; Dieters, U.; Streett, W. B. *J. Chem. Soc., Faraday Trans. 1* **1981**, *77*, 2503.
(3) Chapman, W. G.; Gubbins, K. E.; Jackson, G.; Radosz, M. *Fluid Phase Equilib.* **1989**, *52*, 31.
(4) Chapman, W. G.; Gubbins, K. E.; Jackson, G.; Radosz, M. *Ind. Eng. Chem. Res.* **1990**, *29*, 1709.
(5) Filipe, E. J. M.; Gomes de Azevedo, E. J. S.; Martins, L. F. G.; Soares, V. A. M.; Calado, J. C. G.; McCabe, C.; Jackson, G. *J. Phys. Chem. B* **2000**, *104*, 1315.
(6) Filipe, E. J. M.; Martins, L. F. G.; Calado, J. C. G.; McCabe, C.; Jackson, G. *J. Phys. Chem. B* **2000**, *104*, 1322.
(7) McCabe, C.; Dias, L. M. B.; Jackson, G.; Filipe, E. J. M. *Phys. Chem. Chem. Phys.* **2001**, *3*, 2852.
(8) van Konynenburg, P. H.; Scott, R. L. *Philos. Trans. R. Soc. London, Ser. A* **1980**, *298*, 495.
(9) Streett, W. B.; Calado, J. C. G. *J. Chem. Thermodyn.* **1978**, *73*, 527.
(10) Kleinrahm, R.; Wagner, W. *J. Chem. Thermodyn.* **1986**, *18*, 739.
(11) Theeuwes, F.; Bearman, R. J. *J. Chem. Thermodyn.* **1970**, *2*, 507.
(12) Gil-Villegas, A.; Galindo, A.; Whitehead, P. J.; Mills, S. J.; Jackson, G.; Burgess, A. N. *J. Chem. Phys.* **1997**, *106*, 4168.
(13) Galindo, A.; Davies, L. A.; Gil-Villegas, A.; Jackson, G. *Mol. Phys.* **1998**, *93*, 241.
(14) McCabe, C.; Jackson, G. *Phys. Chem. Chem. Phys.* **1999**, *1*, 2057.
(15) Hicks, C. P.; Young, C. L. *Chem. Rev.* **1975**, *75*, 119−175.
(16) DaPonte, M. N.; Chokappa, D.; Calado, J. C. G.; Clancy, P.; Streett, W. B. *J. Phys. Chem.* **1985**, *89*, 2746−2751.